

# From favorable atomic configurations to supershell structures: a new interpretation of conductance histograms

A. Hasmy<sup>1</sup>, E. Medina<sup>1</sup> and P.A. Serena<sup>1,2</sup>

<sup>1</sup>*Laboratorio de Física Estadística de Sistemas Desordenados, Centro de Física, IVIC, Apartado 21827,*

*Caracas 1020A, Venezuela*

<sup>2</sup>*Instituto de Ciencias de Materiales de Madrid, Consejo Superior de Investigaciones Científicas, Cantoblanco, 28049-Madrid, Spain*

(Sent for publication: August 14th 2000)

## Abstract

Simulated minimum cross-section histograms of breaking Aluminum nanocontacts are produced using molecular dynamics. The results allow a new interpretation of the controverted conductance histogram peaks based on preferential geometrical arrangements of nanocontact necks. As temperature increases, lower conductance peaks decrease in favor of broader and higher conductance structures. This reveals the existence of supershell structures favored by the increased mobility of Al atoms.

PACS numbers: 73.40.Jn,61.16.Ch,73.23.Ad

Electron transport in metallic nanowires having cross-sections formed by few atoms exhibit a rich quantum phenomenology since their characteristic sizes are of the order of the electron Fermi wavelength ( $\lambda_F$ ). Transverse confinement of electrons in the nanocontact region only allows few propagating modes  $N$ , giving rise to quantization of the conductance (assuming perfect transmittance per channel)  $G = N \times G_0$ , where  $G_0 = 2e^2/h$  is the conductance quantum [1]. Although conductance quantization (CQ) was first seen in 2DEG devices [2], the study of this phenomenon in metallic nanocontacts has received much attention because of its technological implications in mesoscopic switching elements and new nanoelectronics devices [3].

Metallic nanocontacts have been built with scanning tunneling microscopy (STM) [4,5], with the Mechanically Controllable Break Junction (MCBJ) method [6,7] as well with two plain macroscopic wires [8]. Nanocontact formation and later breaking are usually carried out in a controlled way using piezoelectric actuators. The conductance evolution is followed by applying a bias voltage to the nanocontact. In general, conductance jumps appear during the nanowire breaking process and correspond to changes of the transmission probability of the propagating modes or sudden variations of  $N$ .

Since every single contact breaking experiment has its own conductance evolution, the study of CQ has been usually addressed from a statistical point of view, elaborating conductance histograms (CH) to get information on the electrical behavior of nanocontacts. In general, CH show a well-defined peaked structure, with higher conductance probabilities close to integer values of  $G_0$ . This trend has been usually interpreted as the evidence of the CQ in different metallic species [5,8,9]. CH have been used to evaluate changes in transport properties when modifying external parameters such as the magnetic field [9], the chemical environment [10], temperature [11,12], or the applied bias voltage [13].

Although CH has become a standard tool to study the electronic transport in metallic nanocontacts, there is no solid theoretical background justifying their use. Any realistic interpretation of CH should take into account that there is a strong coupling between electronic and mechanical properties [14], since conductance and force jumps are correlated, through crystalline rearrangements inside the nanocontact as predicted by Molecular Dynamics (MD) simulations [15]. Therefore, CH give information of the conductance, while the measured histogram weights are related to the stability of a given conductance situation. On the other hand, while for monovalent species an interpretation of CH in terms of number of atoms at the neck seems straightforward [16], for species with higher chemical valence the scenario is less clear. Scheer *et al.* [17] showed that three modes contribute to electron transport in aluminum monoatomic contacts whose conductance is close to  $G_0$ . Similar results for Pb and Nb demonstrate the existence of a correspondence between valence and the number of conduction channels participating in one-atom contacts [17,18]. For Al, CH constructed from many MCBJ experiments [19] clearly show peaks close to  $G/G_0 \sim 0.8$ ,  $\sim 1.8$ ,  $\sim 3.0$ , and  $\sim 4.0$  at  $T=4K$ . A quite similar experimental series of peaks for Al has been reported recently [20]. These results have been used to reconsider the role of CH to indicate CQ features. In particular, it has been suggested that peaks in aluminum CH originate in favorable atomic configurations appearing during nanocontact stretching [19,20].

In the past, within the framework of the free-electron model together with conductance calculations, theoretical CH have been obtained by considering a simplified *ad-hoc* nanowire dynamics [21]. A realistic description of the dynamics of the metallic nanowires breakage

can be obtained by means of first-principles calculations [22]. Other authors used classical Molecular Dynamics accompanied with conductance calculations [23–25]. However, to construct CH, both approaches are impracticable because of the prohibitive computational cost.

In this letter, we have adopted a different perspective. Our goal is to construct *atomic configuration histograms* of the neck instead of conductance histograms. In this way we will be able to know whether there are favorable atomic configurations behind the peaked structure obtained in CH. We have studied the atomic configuration histograms of aluminum, a trivalent metal, which shows a well defined and reproducible peaked structure [19,20]. For the statistical study of breaking nanocontacts we performed MD simulations using the embedded atom method (EAM) [26] as in previous works [15,24]. In particular, we have used state-of-the-art many-body EAM interatomic potentials for aluminum able to fit bulk and surface properties [27]. Simulations were carried out in a wide range of temperatures (4K-450K) in order to assess the influence of temperature  $T$  on the configuration histograms. The temperature is controlled during the simulation using conventional scaling of velocities.

As starting point of our MD simulation we consider a parallelepiped supercell containing 1008 Al atoms ordered following a fcc crystallographic structure. The lattice constant is taken to be equal to the experimentally measured value (4.05 Å). Aluminum atoms were initially distributed in 18 layers perpendicular to the (111) direction containing 56 atoms each [see Fig.1a (left) for illustration]. The direction (111) ( $z$  axis in our simulation) corresponds to that in which the contact will be elongated until breaking, although we also have considered other orientations discussed below. Each single MD simulation is carried out following three stages. First, we relax the initial bulk-like ordered system for 2000 iterations, imposing periodic boundary conditions (PBC) in the  $x$  and  $y$  directions of the sample. The time interval per iteration step in all our simulations is  $dt = 10^{-14}$  sec. At the end of this equilibration step the system undergoes a relaxation characterized by a contraction along the  $z$  axis. In the final thermally equilibrated structure two bi-layer slabs are defined at the top and bottom of the supercell. All atomic positions inside these slabs are frozen during subsequent MD stages, defining the bulk support of the nanocontact during the breaking process. In a second stage, the system is again thermally equilibrated during 3000 iterations, but now PBC are preserved only in the  $x$  and  $y$  directions of the frozen slabs. The other atoms, defining a free nanowire evolve to reach a new equilibrium configuration. For temperatures higher than 450K, we found that we are not able to stabilize the nanowire geometry, which spontaneously breaks. This is consistent with the decrease of the melting temperature noted for metallic nanowires as their radius decreases [28]. The third stage corresponds to the nanowire stretching, separating both supporting frozen slabs at a constant velocity of  $2 \times 10^{-4}$  Å per iteration step. The full determination of atomic positions during the elongation process allows the determination of an effective surface for the nanocontact and a minimum cross-section  $S_N$  time evolution [25]. The quantity  $S_N$  is computed as in ref. [25] (in units of numbers of atoms) and is approximately equal to the Sharvin conductance of the nanocontact in units of  $G_0$ . In order to reduce the computational effort, we evaluate  $S_N$  each 10 MD iterations.

An illustration of the nanocontact evolution during elongation  $\Delta d$  is depicted in Fig. 1a. Fig. 1b shows the evolution of  $S_N$  as a function of  $\Delta d$  for four different realizations (i.e. each relaxed parallelepiped gives rise to a different nanowire evolution until breaking

takes place). The jumps in  $S_N$  curves are correlated with the jumps of the resulting force on the frozen slabs as observed previously [4,25]. By accumulating conductance traces we can construct minimum cross-section histograms  $H(S_N)$ . The number of single nanowire breaking realizations  $N_s$  considered is such that the obtained histogram peak structures are unchanged under further averaging (see Fig. 1c). In our calculations we have found that  $N_s = 100$  provides a reliable  $H(S_N)$  curve.

In Fig. 2 we plot the histogram  $H(S_N)$  for three different temperatures. For low temperatures ( $T = 4\text{K}$ ) it is clear that  $H(S_N)$  presents a well-defined peaked structure with maxima located at  $S_N = 1, 2, 3, 4$ , etc. Therefore, *the statistics of the nanocontact at the narrowest section exposes favorable atomic configurations during its stretching*. Although our histograms do not contain direct information on conductance, the resemblance with experimental histograms [19,20] is remarkable. Assuming that one Al atom provides a conductance close to  $G_0$  (including components from three different channels) the interpretation of  $H(S_N)$  as a conductance histogram is close to the observed results.

For increasing temperatures, we found that the histogram dramatically changes losing its peaked features for low  $S_N$  values, whereas a different structure appears for high  $S_N$  values. This trend is similar to that found in Na conductance histograms reflecting the appearance of supershell high stability structures [12]. In our case, the temperature needed to find such supershell configurations is higher than in Na wires due to the higher cohesion energy of Al (1.13 and 3.36 eV in Na and Al bulk, respectively). Although the explored region only corresponds to  $S_N \leq 30$  the presence of peaks at  $S_N \simeq 5, 8, 12, 17, 24$  is evident. The shell structure becomes observable at higher temperatures because of the increased mobility of the atoms. This allows the system to explore many atomic configurations in order to efficiently find a suitable local energy minimum.

By inspecting Fig. 2 (where  $H(S_N)$  is shown in a range similar to that used in experimental situations), it is clear that temperature has a dramatic effect on the favorable geometrical configurations. The higher the temperature the larger the background structure, giving rise to a histogram with a less defined peak structure. In particular it is very striking that the peak at  $S_N = 1$  is still well defined at  $T = 300\text{K}$  while the peak  $S_N = 2$  decreases its relative weight with respect to those found in  $S_N = 3$  and 4, in comparison to the 4K case. At  $T=450\text{K}$  the  $S_N = 1$  peak almost vanishes and the broad structure around  $S_N = 5$  appears, whereas intermediate peaks at  $S_N = 2, 3$  and 4 disappear. Although these predictions correspond to cross-section histograms, we believe a similar behavior is to be expected in true CH.

In actual experiments the nanowire orientation is not well defined, and the histogram would contain components coming from different nanowire orientations. In order to analyze these effects we have studied the histograms  $H(S_N)$  at  $T = 4\text{K}$  for two other orientations of the stretching direction: (011) and (001). These results are depicted in Fig. 3. It is worth noticing that the histograms have now a more complicated structure but also reflect the presence of favorable atomic configurations. We can then expect that in experiments the histograms can be understood in terms of a combination of the histograms appearing in Fig. 3. However it is clear that a structure with peaks at  $S_N = 1$  and 2 should be present. For  $S_N \geq 3$  the peaked structure should become less clear and would depend on the experimental conditions (as it happens when comparing two different experimental conductance histograms in Al [19,20]). Another relevant observation is that for less stable configurations, as those considered when stretching along (011) and (001) directions, the

shell structure tends to appear at lower temperatures [see, for instance, the peak at  $S_N = 5$  formed in the (011) case]. Thus, orientation effects will also contribute in bringing out supershell effects.

In conclusion, we have obtained, for the first time, minimum cross-section histograms for Al nanowires breaking MD simulations using state-of-the-art EAM potentials to describe Al-Al interactions. At low temperatures we found that there exist favorable atomic arrangements as suggested some time ago by experimentalist [19,20]. This provides a new way to interpret experimental conductance histograms on the basis of MD simulations. For increasing temperatures, the system is able to explore more atomic configurations where low conductance regions show less structure and appearing well defined high stability regions for higher conductance values appear, as reported for Na [12]. In the low conductance region it is found that at  $T = 300\text{K}$  the histogram peak at  $S_N = 2$  decreases its relative weight with respect the peak  $S_N = 3$ . That is, at 4K the peak height sequence is 1, 2, 3, 4 whereas at 300K the sequence change to 1, 4, 3, 2. For  $T=450\text{K}$  the peak at  $S_N = 1$  almost vanishes, and the presence of supershell structure becomes evident. Finally, for other nanowire stretching directions in the low temperature regime we also found that there exist favorable configurations, although the histogram presents a more complex structure. However peaks at  $S_N = 1$  and 2 remain. Nanowires with lower stability tend to form the supershell structure at lower temperatures than those with high initial stability.

We acknowledge J.J. Sáenz, P. García-Mochales, C. Urbina, R. Paredes, J.R. Villarroel, and A. García-Martín, for helpful discussions. This work has been partially supported by the CSIC-IVIC researchers exchange program and the Spanish DGICYT (MEC) through Project PB98-0464.

## REFERENCES

- [1] R. Landauer, Z. Phys. B - Condens. Matter **68**, 217 (1987); J. Phys. Condens. Matter **1**, 8099 (1989).
- [2] D. A. Wharam *et al.*, J. Phys. C **21**, L209 (1988); B. J. van Wees *et al.*, Phys. Rev. Lett. **60**, 848 (1988).
- [3] *Nanowires*, edited by P.A. Serena and N. García, NATO ASI Series E, Vol. 340 (Kluwer, Dordrecht, 1997).
- [4] J. I. Pascual *et al.*, Phys. Rev. Lett. **71**, 1852 (1993); N. Agraït, J.G. Rodrigo, and S. Vieira, Phys. Rev. B **47**, 12345 (1993).
- [5] L. Olesen *et al.*, Phys. Rev. Lett. **72**, 2251 (1994); Phys. Rev. Lett. **74**, 2147 (1995); J.L. Costa-Krämer *et al.*, Phys. Rev. B **55**, 5416 (1997).
- [6] C.J. Muller, J. M. van Ruitenbeek, and L. J. de Jongh, Phys. Rev. Lett. **69**, 140 (1992).
- [7] J.M. Krans *et al.*, Phys. Rev. B **48**, 14721 (1993); Nature (London) **375**, 767 (1995); Phys. Rev. Lett. **74**, 2146 (1995).
- [8] J.L. Costa-Krämer *et al.*, Surf. Sci. **342**, L1144 (1995); Erratum in Surf. Sci. **349**, L138 (1996).
- [9] J.L. Costa-Krämer, Phys. Rev. B **55**, R4875 (1997); H. Oshima and K. Miyano, Appl. Phys. Lett. **73**, 2203 (1998)
- [10] C. Z. Li and N. J. Tao, Appl. Phys. Lett. **72**, 894 (1998); C. Shu *et al.*, Phys. Rev. Lett. **84**, 5196 (2000).
- [11] C. Sirvent *et al.*, Physica B **218**, 238 (1996).
- [12] A.I. Yanson, I.K. Yanson, and J.M. van Ruitenbeek, Nature (London) **400**, 144 (1999); Phys. Rev. Lett. **84**, 5832 (2000).
- [13] H. Yasuda and A. Sakai, Phys. Rev. B **56**, 1069 (1997); K. Itakura *et al.*, Phys. Rev. B **60**, 11163 (1999).
- [14] G. Rubio, N. Agraït, and S. Vieira, Phys. Rev. Lett. **76**, 2302 (1996).
- [15] U. Landman *et al.*, Science **248**, 454 (1990).
- [16] H. Ohnishi *et al.*, Nature (London) **395**, 780 (1998).
- [17] E. Scheer *et al.*, Phys. Rev. Lett. **78**, 3535 (1997); Nature (London) **394**, 154 (1998).
- [18] B. Ludoph *et al.*, Phys. Rev. B **61**, 8561 (2000).
- [19] A. I. Yanson and J. M. van Ruitenbeek, Phys. Rev. Lett. **79**, 2157 (1997).
- [20] B. Ludoph and J.M. van Ruitenbeek, Phys. Rev. B **61**, 2273 (2000).
- [21] J.A. Torres and J.J. Sáenz, Phys. Rev. Lett. **77**, 2245 (1996); T. López-Ciudad *et al.*, Surf. Sci. **440**, L887 (1999); J. Bürki *et al.*, Phys. Rev. B **60**, 5000 (1999).
- [22] A. Nakamura *et al.*, Phys. Rev. Lett. **82**, 1538 (1999).
- [23] T.N. Todorov and A.P. Sutton, Phys. Rev. Lett. **70**, 2138 (1993); Phys. Rev. B **54**, R14234 (1996); M. Brandbyge, M. R. Sorensen, and K.W. Jacobsen, Phys. Rev. B **56**, 14956 (1997).
- [24] H. Mehrez and S. Ciraci, Phys. Rev. B **56**, 12632 (1998); A. Buldum *et al.*, Phys. Rev. B **57** 2468 (1998).
- [25] A.M. Bratkovsky, A. P. Sutton, and T.N. Todorov, Phys. Rev. B **52**, 5036 (1995); M.R. Sorensen, M. Brandbyge, and K.W. Jacobsen, Phys. Rev. B **57**, 3283 (1998).
- [26] M.S. Daw, S.M. Foiles, and M.I. Baskes, Mater. Sci. Rep. **9**, 251 (1993).
- [27] Y. Mishin *et al.*, Phys. Rev. B **59**, 3393 (1999).
- [28] O. Gülseren, F. Ercolessi, and E. Tosatti, Phys. Rev. B **51**, R7377 (1995).

## FIGURES

FIG. 1. (a) Typical nanocontact configurations during the elongation of the sample. (b) Minimum cross-section  $S_N$  evolution for four different Al nanowires at  $T = 4\text{K}$ . The stretching direction is parallel to the (111) direction, and the arrows indicate the corresponding  $S_N$  for each configuration. (c) Minimum cross-section histograms  $H(S_N)$ . Dark gray, gray and black curves correspond to histograms obtained with different number of realizations (35, 70 and 100, respectively).

FIG. 2. Minimum cross-section histograms  $H(S_N)$  for stretching of Al nanowires along the (111) direction at  $T=4\text{K}$ , 300K, and 450K. The right panel is a zoom of the range  $0 \leq S_N \leq 8$ . The curves are normalized to the number of single breaking events (100 per temperature value).

FIG. 3. Comparison of the minimum cross-section histograms  $H(S_N)$  of aluminum nanowires at  $T = 4\text{K}$  stretching along three different orientations (111), (011) and (001). The last two histograms are constructed with 70 breaking events and nanocontacts contain 1000 and 980 atoms, respectively. All histograms are normalized to the number of realizations

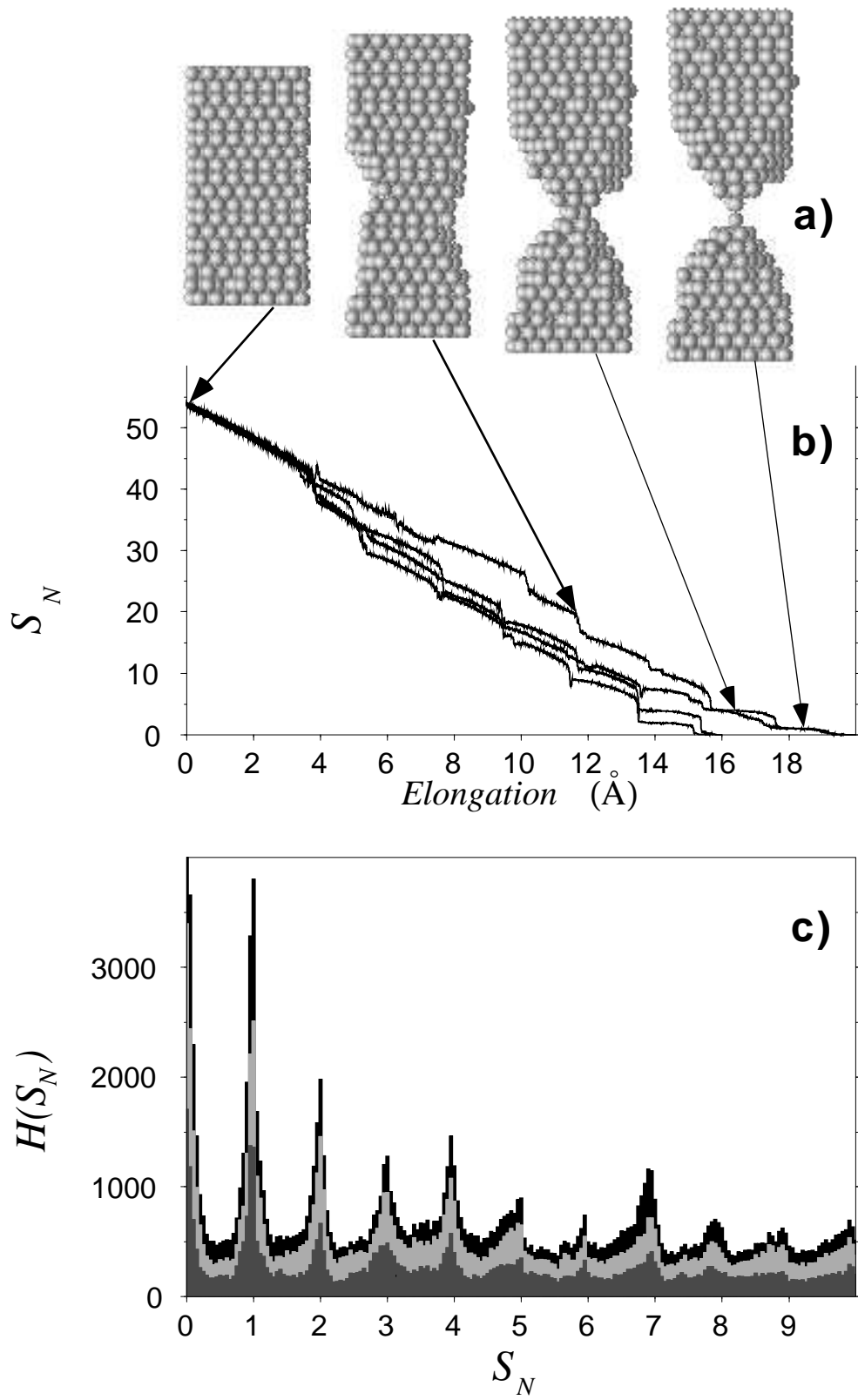


FIG. 1



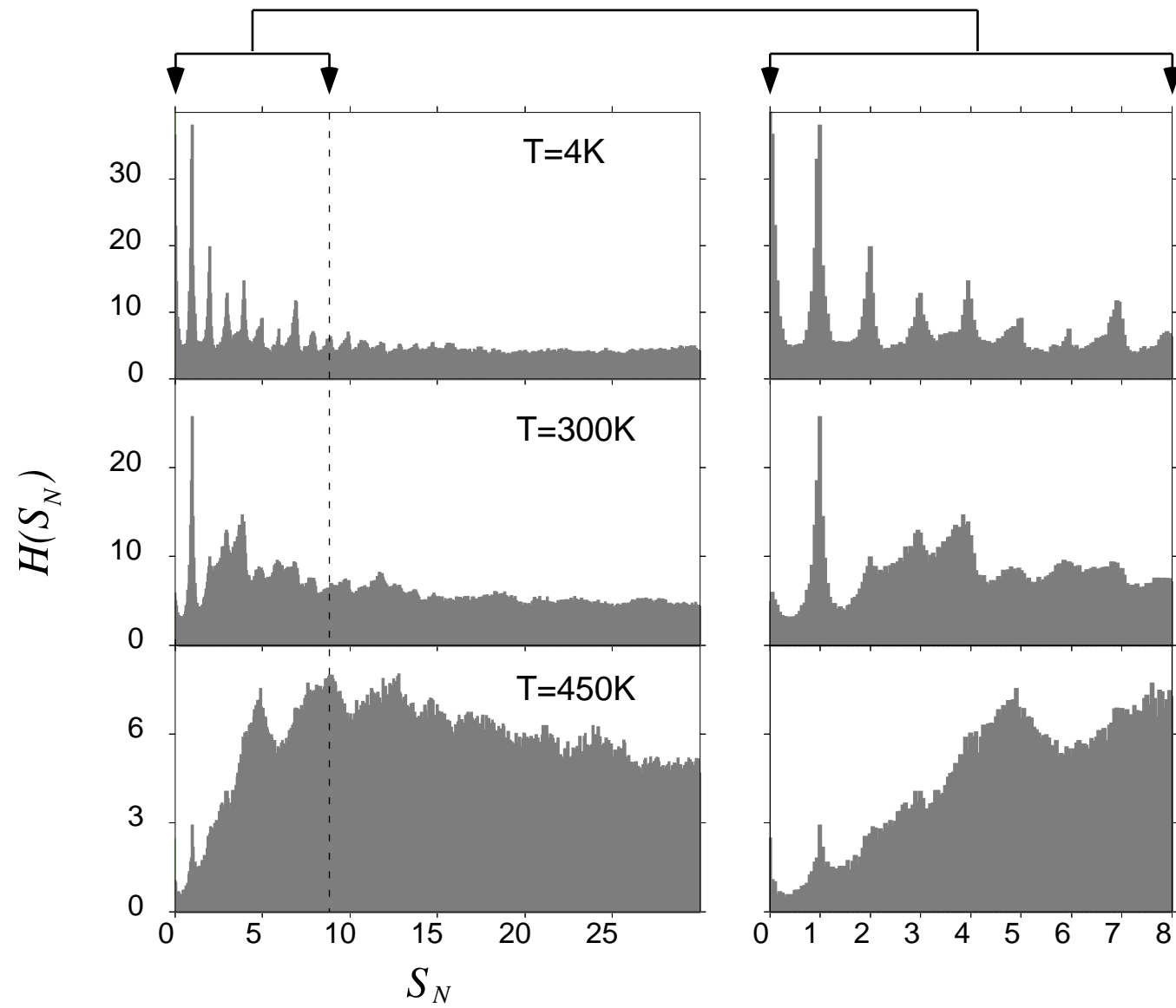


FIG. 2

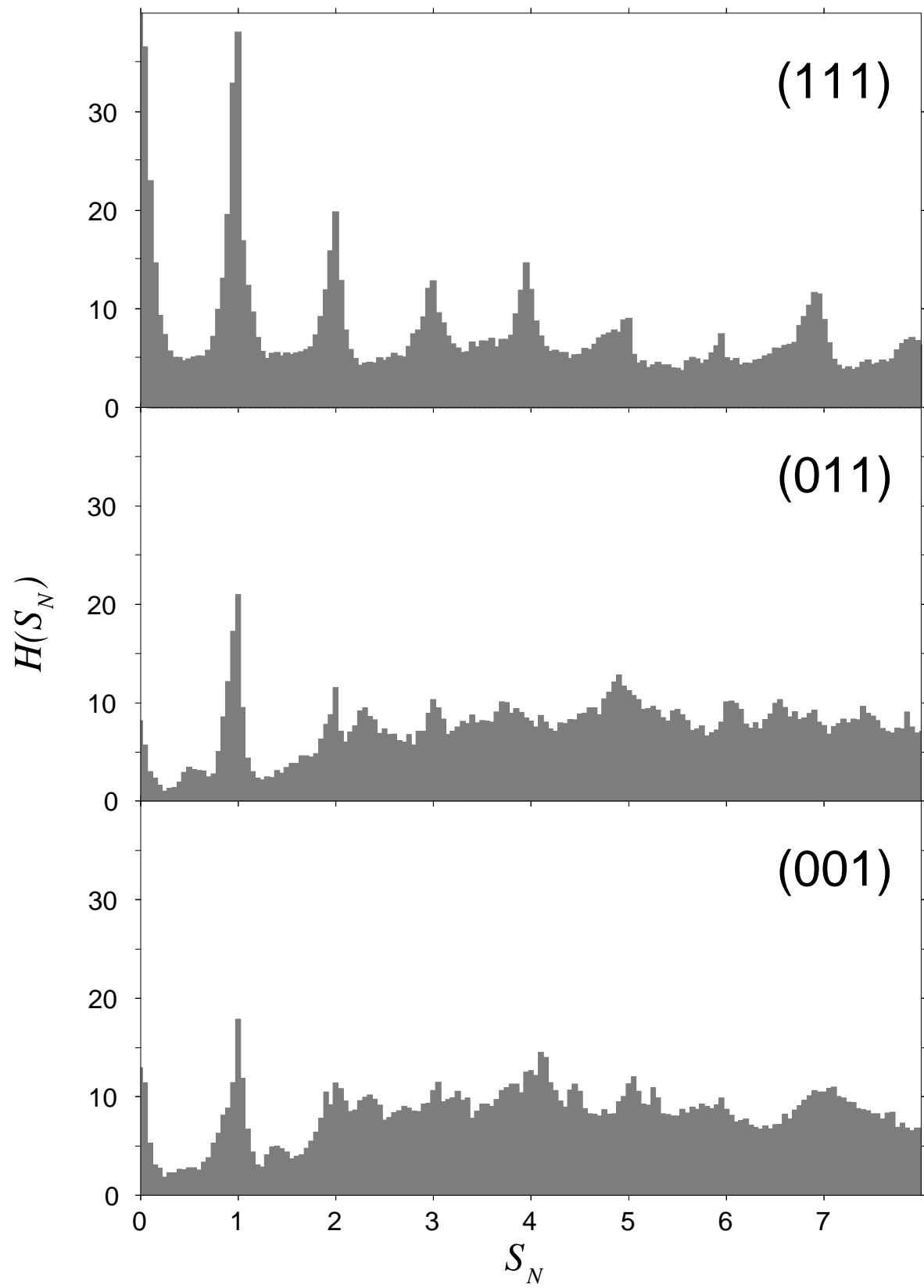


FIG. 3